LWT - Food Science and Technology 169 (2022) 114030

Contents lists available at ScienceDirect

LWT

journal homepage: www.elsevier.com/locate/lwt

LMOF serve as food preservative nanosensor for sensitive detection of nitrite in meat products

Siyang Deng [a,d], Huan Liu [b,c,**], Chunhui Zhang [a,*], Xinting Yang [b,c], Christophe Blecker [d]

[a] Key Laboratory of Agro-Products Processing, Ministry of Agriculture and Rural Affairs, Institute of Food Science and Technology, Chinese Academy of Agricultural Sciences, Beijing, 100193, China
[b] Research Center for Information Technology, Beijing Academy of Agricultural and Forestry Sciences, Beijing, 100097, China
[c] National Engineering Research Center for Information Technology in Agriculture, Beijing, 100097, China
[d] Unit of Food Science and Formulation, University of Liège, Gembloux Agro-Bio Tech, Passage des Déportés, 2B, 5030, Gembloux, Belgium

ARTICLE INFO

Keywords:
Nitrite
Rhodamine 6G
Luminescent metal organic framework
Meat products

ABSTRACT

Nitrite (NO_2^-) is widely present in meat products as a vital food preservative, while excessive nitrite is a serious carcinogen to human beings, developing a sensitive and selective nitrite detection method is of great significance for food safety. Herein, a novel luminescent metal organic framework (LMOF) (Rh6G@MOF-5) is prepared through a facile one-pot synthesis as a fluorescent turn-off sensor for NO_2^- determination. Upon exposure to NO_2^-, significant fluorescence intensity decreases linearly along with NO_2^-concentration in the range of 0–200 μmol/L and the detection limit is estimated to be 0.2 μmol/L. The developed nanocomposite has been shown to be an ultrasensitive and selective nanoprobe for detecting NO_2^- in meat products, with recoveries ranging from 96.1% to 103.2% with the RSDs less than 4%. Rh6G@MOF-5 nanoprobe offers insight into the fabrication of MOF-based sensors with low cost and convenient operation in analyte detection field.

1. Introduction

Nitrite (NO^{2-}) has been used as an essential food additive (such as chromogenic agents, flavoring agents and preservatives) in the food industry that can improve color, texture, and storage stability (Nam et al., 2018; Wang et al., 2016). Nevertheless, their application is controversial since excessive intake of nitrite in food would cause a serious health threat to the public. Nitrite can be converted to *N*-nitrosamines when reacted with secondary amines and amides, which have been identified as potential carcinogens and mutagens (Canbay, Şahin, Kıran, & Akyilmaz, 2015; Kilfoy et al., 2011; Santarelli et al., 2010). Therefore, excessive consumption of nitrites in the human body will lead to numerous diseases such as esophageal cancer, infant methemoglobinemia and central nervous system deficiencies, etc (Brender et al., 2004; Greer & Shannon, 2005; Maia & Moura, 2014; Zhou, Anwar, Zahid, Shostrom, & Mirvish, 2014). Due to these toxic effects, the establishment of an efficient, facile, and sensitive method to detect nitrite is of great significance in food products, especially for meat products.

Conventional and reliable detection methods have been reported for nitrite determination, including capillary electrophoresis (CE) (Lee, Shiddiky, Park, Park, & Shim, 2008; Merusi, Corradini, Cavazza, Borromei, & Salvadeo, 2010), chromatography (Li, Meininger, & Wu, 2000; Pérez-López et al., 2016), electrochemical methods (Liu et al., 2017; Wan, Zheng, Wan, Yin, & Song, 2017) and so on. Although these techniques have been widely used in the past, most of them have several drawbacks, including expensive instrumentation, laborious and time-consuming procedures, which have limited their wide utilization. In comparison, spectrofluorimetric analysis is a preferred selection for nitrite detection due to its high sensitivity, convenience, easy operation, low-cost, and ability to be used for on-line or visual on-site analysis (Hu et al., 2019; Zheng, Liang, Li, Zhang, & Qiu, 2016). Therefore, it is of significance to fabricate effective probes for nitrite recognition based on the fluorescent technique to work in an aqueous system.

Metal organic frameworks (MOFs), rising as a new class in microporous hybrid crystalline materials, are constructed by the coordination of metal centers and organic ligands via a self-assembly approach (Sahiner, Demirci, & Yildiz, 2017), and can be applied in various fields for their superior structures and physicochemical properties (such as high porosity, uniform nanoscale cavities, adjustable compositions, and functional surfaces) (Furukawa, Cordova, O'Keeffe, & Yaghi, 2013). As a

* Corresponding author.
** Corresponding author. Research Center for Information Technology, Beijing Academy of Agricultural and Forestry Sciences, Beijing, 100097, China.
E-mail addresses: liuhuan@nercita.org.cn (H. Liu), dr_zch@163.com (C. Zhang).

https://doi.org/10.1016/j.lwt.2022.114030
Received 15 July 2022; Received in revised form 20 September 2022; Accepted 24 September 2022
Available online 27 September 2022

novel class of exciting MOF materials, LMOF-based sensors are gaining interest as their nanoscale cavities and three-dimensional (3D) network architectures, which act as micro-reactors, provide adequate space for the identification and selective recognition of objective targets through signal amplification (Guo, Liu, Kong, Chen, Liu, et al., 2019). Acting as host matrices, MOFs can be viewed as unique platforms for stabilizing and confining functional groups, resulting in specific behavior inside the defined pore environments. Aggregation-caused quenching (ACQ) can also be limited through immobilizing organic dyes into the pores of MOFs (Guo, Liu, Kong, Chen, Liu, et al., 2019). Thus, LMOF composites introduce the organic dyes into MOFs through a "ship in a bottle" way and combine the advantages of MOFs' crystalline benefit with the high luminous efficiency of luminescent genes, which have attracted extensive attention due to their unique ability to recognize specific analytes (Ye et al., 2019). Accordingly, this prompted us to synthesis a superior LMOF that can be used to impede large-sized interferents and thus improve their specificity toward nitrite sensing, while also reducing the ACQ effect of the fluorescent dye itself. In the last few years, LMOFs have been probed for important applications such as temperature sensing, toxic or less environmentally friendly molecular (antibiotics, pesticides, metal ions, explosive, and so on) detecting (Let, Samanta, Dutta, & Ghosh, 2020; Liu et al., 2019; Wang & Yan, 2019). However, to the best of our knowledge, such kind of LMOF based sensor for detection of nitrite in meat products have rarely been reported so far.

In this work, we prepared a high-quality LMOF based on organic dye and MOF hybrid materials via a facilely solvothermal synthesis approach, in which rhodamine 6G (Rh6G) was incorporated into the porous crystalline Zn-MOF (MOF-5) serving as a nitrite ion detecting sensor (Scheme A). The optimized Rh6G@MOF-5 composite exerts a uniformly nanosized distribution and excellent MOF-5 porosity, and its suspension emits a distinctive yellow-green emission at 545 nm. Moreover, compared with free Rh6G dye, the LMOF in this study not only kept Rh6G molecules away from the ACQ effect but also exhibited higher photostability and longer fluorescence lifetime. These results showed that the Rh6G@MOF-5 could enhance the sensing ability towards nitrite ion through a "turn-off" fluorescence response in view of the inner filter effect (IFE) and electron-withdrawing effect. Moreover, the fascinating LMOF was successfully used to detect nitrite ions with satisfactory results in meat products' system.

2. Materials and methods

2.1. Chemicals and materials

Zinc nitrate hexahydrate ($Zn(NO_3)_2{\cdot}6H_2O$), 1,4-benzenedicarboxylic acid (H_2BDC), *N, N*-Dimethylformamide (DMF) and rhodamine 6G (Rh6G) were purchased from Aladdin reagent company (Shanghai, China). Sodium nitrite ($NaNO_2$) and aqueous solutions of interference ions (NO_3^-, SO_4^{2-}, CO_3^{2-}, Cl^-, K^+, Na^+, Ca^{2+}, Mg^{2+}, Pb^{2+}, Zn^{2+}, Cu^{2+}, Mn^{2+}, Fe^{2+}, Fe^{3+}, Al^{3+}, $H_2PO_4^-$ and HPO_4^{2-}) were supplied by Macklin Biochemical Co., Ltd. (Shanghai, China). And all chemicals and solvents were of analytical grade and used without further purification.

2.2. Instrumentation

The fluorescence spectra of the sensors were recorded with a fluorescence spectrometer (Hitachi F-7000, Tokyo, Japan), the integration time was set at 0.05 s and the emission and excitation slit widths were all 5 nm. The ultraviolet–visible (UV–Vis) spectra were scanned by a UV–Vis spectrophotometer (Hach DR6000, Loveland, USA) in the wavelength range of 300 nm–600 nm with a step size of 2 nm. Powder X-ray diffraction (PXRD) patterns were performed using the Panalytical X-ray Diffractometer Smartlab-9kW (Tokyo, Japan) employing Cu Kα radiation ($\lambda = 1.5406$ Å, 40 kV, 250 mA) in the 2θ range of 2–50°. Fourier transform infrared (FT-IR) spectra were obtained using a FT-IR spectrophotometer (Thermo Scientific Nicolet IS5, USA) within the 4000-400 cm^{-1} region. Scanning electron microscopy (SEM) images were obtained by a field-emission scanning electron microscope (FEI Inspect F50, USA). The fluorescence lifetimes were collected using the FLS1000 series of fluorescence spectrometers (Edinburgh FS5, Livingston, UK).

2.3. Synthesis of Rh6G@MOF-5

The synthesis of Rh6G@MOF-5 porous material was based on previous reports using a solvethermal method with some slight modification (Guo, Liu, Kong, Chen, Wang, et al., 2019). In brief, Zn $(NO_3)_2{\cdot}6H_2O$ (2 mmol) and H_2BDC (1 mmol) were dissolved in 40 mL of DMF and the mixture was treated with ultrasound for about 30 min. Then, various amounts of Rh6G were added into the above solution, with 30 min of sonication for each addition. Then, the mixture was placed in a 200 mL polytetrafluoroethylene stainless steel reactor and heated in an oven at 120 °C for 24 h. After the reaction was completed and the polytetrafluoroethylene stainless steel reactor cooled to room temperature, solid

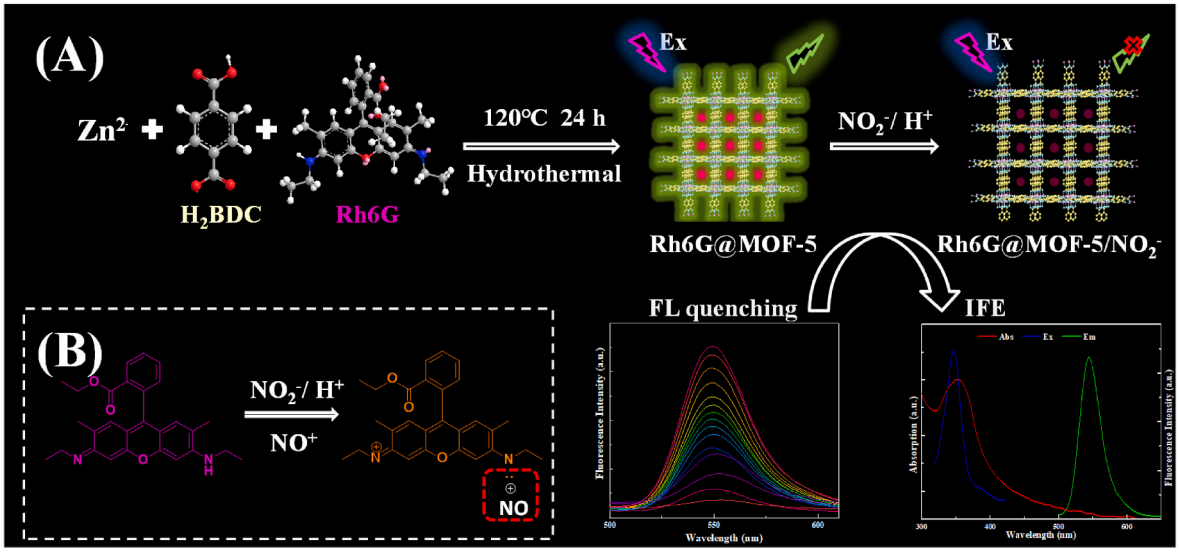

Scheme 1. Schematic illustration for the construction of Rh6G@MOF-5 (A) and the possible mechanism for detection of nitrite (B).

products were collected through centrifugation (8000 rpm/min, 5 min) and washed more than three times with DMF and methanol to remove unreacted ligand. Finally, the dye-encapsulated MOF composites (Rh6G@MOF-5) were dried at 120 °C in a vacuum oven for 12 h to obtain some solid powders. The control MOF-5 synthesis step was the same as above, except that no Rh6G molecules were added.

2.4. Quantitative detection of nitrite

To detect the nitrite response of the system, a series of different concentrations of nitrite aqueous solutions (0–300 μmol/L) were prepared and the detection of nitrite was performed in an acidic environment at room temperature. Firstly, 10.0 mg Rh6G@MOF-5 powder was dispersed in 25 mL deionized water and magnetically stirred for 20 min to form standard stock solution of Rh6G@MOF-5. Subsequently, 100 μL of Rh6G@MOF-5 stock solution was mixed with 800 μL of HCl solution (0.4 mol/L), then incrementally added 100 μL different concentrations of freshly prepared nitrite aqueous solution to the above mixture. The resulting suspension was mixed thoroughly before recording the fluorescence emission spectra with excitation at 350 nm. Furthermore, all the following peaks were recorded more than three times in order to guarantee the experimental reliability.

2.5. Selectivity measurement of nitrite

The selectivity of Rh6G@MOF-5 probe to nitrite was examined via adding some other interferences or common ions which coexist with nitrite in meat products, including NO_2^-, NO_3^-, SO_4^{2-}, CO_3^{2-}, Cl^-, K^+, Na^+, Ca^{2+}, Mg^{2+}, Pb^{2+}, Zn^{2+}, Cu^{2+}, Mn^{2+}, Fe^{2+}, Fe^{3+}, Al^{3+}, $H_2PO_4^-$, and HPO_4^{2-}, respectively, in a manner similar to that of nitrite.

2.6. Analysis of nitrite in meat products

Meat products (including sausage, bacon, pork ham, beef ham, stewed beef, and braised chicken) were obtained from a local supermarket (Beijing, China). The method of NO_2^- extraction in meat samples was implemented on the basis of the People's Republic of China National Food Safety Standard (GB 5009.33–2016). 5.0 g of crushed sample was weighed and placed in a 250 mL glass conical flask with a stopper, followed by 12.5 mL of saturated borax solution (50 g/L) and approximately 150 mL of distilled water at 70 °C. After that, the conical flask was heated in a boiling water bath for 15 min before being cooled to room temperature. To transfer the extracted liquid into a 200 mL volumetric flask, put in 5 mL of potassium ferrocyanide (106 g/L), 5 mL of zinc acetate (220 g/L) and distilled water in order, then shake well. The homogenate was placed for 30 min then filtered using filter paper to remove unsolvable and useless substances. Finally, 30 mL of initial filtrate was discarded, and the final filtrate obtained was preserved in the refrigerator at 4 °C for later use.

2.7. Statistical analysis

The nitrite detection results are expressed as the mean values ± standard deviations by using Statistix 8.1 software package (Analytical Software, St Paul, MN, USA). In addition, all graphs were constructed using Origin 2021.

3. Results and discussion

3.1. Basic characterizations of Rh6G@MOF-5

The morphological and structural characterization of Rh6G@MOF-5 was determined by the following tests. Firstly, the PXRD was performed to verify the successful preparation of the Rh6G@MOF-5 composite. As shown in Fig. 1A, the prepared MOF-5 and Rh6G@MOF-5 exhibited similar diffraction peaks to the simulation one, indicating that the prepared MOFs presented an intact structure and showed high crystallinity. The encapsulated Rh6G had a negligible effect on the MOF-5 lattice. In addition, analogous XRD sharp diffraction peaks of MOF-5 and Rh6G@MOF-5 demonstrated that Rh6G dyes were encapsulated into the cavity instead of physically aggregated and adsorbed on the surface of the MOF-5 crystal. A similar phenomenon was also documented by Ye et al. (2019), who showed that the encapsulating of 5-aminofluorescein through the "ship in a bottle" approach only gave rise to color change without morphology change in parent MOF-801.

The FT-IR spectra of MOF-5 and Rh6G@MOF-5 composites were also characterized to determine the molecular structure (Fig. 1B). According to the literature, the observed peaks at 530 cm^{-1} and 750 cm^{-1} resulted

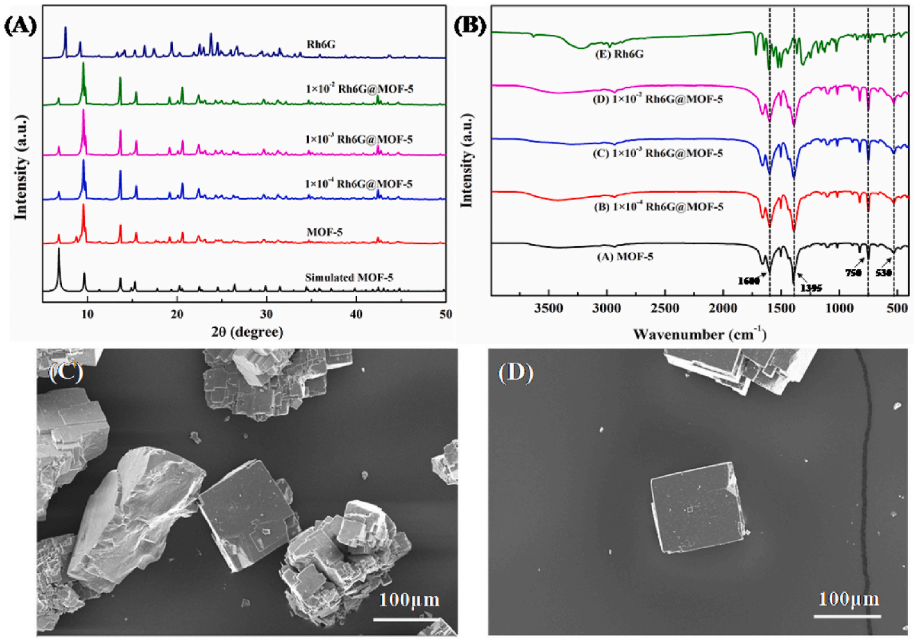

Fig. 1. (A) PXRD patterns of simulated MOF-5, synthesized MOF-5, 10^{-4} Rh6G@MOF-5, 10^{-3} Rh6G@MOF-5, 10^{-2} Rh6G@MOF-5 and Rh6G. (B) FT-IR spectra of MOF-5, 10^{-4} Rh6G@MOF-5, 10^{-3} Rh6G@MOF-5, 10^{-2} Rh6G@MOF-5 and Rh6G. SEM images of synthesized MOF-5 (C) and Rh6G@MOF-5(D).

from the stretching vibration of Zn–O and C–H in the tetrahedral Zn_4O crystal cluster of MOF-5, respectively (Petit & Bandosz, 2009). The characteristic absorption peaks of MOF-5 nanocrystals situated at 1395 cm^{-1} and 1600 cm^{-1} were in line with the symmetrical and asymmetric stretching vibrations of the carboxyl group, which is one of the principal functional groups of H_2BDC ligands (Hu, Yang, Wang, & Duan, 2021). The results were in agreement with the MOF-5's structure. Furthermore, no visible difference could be found in the FT-IR spectra between MOF-5 and Rh6G@MOF-5, and no blue or red shift after Rh6G encapsulation, illustrating that the Rh6G had successfully enclosed into the pores of MOF-5 and the organic dye in nanocrystals did not affect the building of MOF-5. Besides, the characteristic peaks of Rh6G were not observed in Rh6G@MOF-5, further indicating that Rh6G fluorescein was localized inside the pores of MOF-5. This is consistent with PXRD analysis results.

As revealed by SEM images (Fig. 1C and D), the shape of the obtained MOF-5 and Rh6G@MOF-5 presented the "cube sugar-like" morphology, similar results have also been reported by Guo, Liu, Kong, Chen, Wang, et al. (2019). As we can see, they all presented good dispersibility, uniform size, and no significant morphological differences. And the Rh6G@MOF-5 was a regular crystal combined with some nanoscale sub-crystals. The morphology of all Rh6G@MOF-5 composites matched well with the pure MOF-5, further proving that the crystal structure of MOF was not affected by the Rh6G-loading process regardless of the concentrations of Rh6G dye molecules (Fig. S1). This appearance allows us to dominate the grain size of the proposed Rh6G@MOF-5 so long as the morphology of the original MOF-5 can be effectively mediated in an appropriate way (Ye et al., 2019). All these above results illustrate that Rh6G dye molecules have been successfully incoporated into parental MOF-5 and the skeleton structure of MOF-5 is maintained.

3.2. Photoluminescence studies of Rh6G@MOF-5

According to above characterization of synthesized Rh6G@MOF-5, Rh6G dye molecules have been successfully incorporated into the cavities of MOF-5 with well interspersing because of the uniform pore confinement effect. The digital photographs of Rh6G, Rh6G mixed with MOF-5, MOF-5 and Rh6G@MOF-5 with different Rh6G concentrations under visual light and 365 nm UV light were taken for observation with the naked eye (Fig. 2A). In addition, fluorescence spectra were recorded in order to optimize the loading amount of fluorescent dye in MOF-5 (Fig. S2 and Fig. S3). It should be emphasized that no fluorescence emission was obtained in the solid-state Rh6G molecules for the ACQ effect, which usually exists in aggregated dye molecules due to non-radiative energy transfer (Fig. S2A). Furthermore, the mechanically ground mixture of Rh6G and MOF-5 had no significant improvement effect as well (Fig. S2B). As shown in Fig. 2A, with the rise of the Rh6G additions (range from 0 to 1×10^{-2} mol/L), the color of Rh6G@MOF-5 changed from white to faint pink to pink to orange, and the corresponding fluorescence color of Rh6G@MOF-5 represented blue, green, strong yellow, and weaker yellow color, respectively, matching well with the fact that an increasing number of Rh6G dye molecules were loaded into the original MOF-5. Furthermore, seen from the calculated Commission Internationale de L'Eclairage (CIE) chromaticity coordinates diagram, they are (0.161, 0.109), (0.297, 0.395), (0.405, 0.496) and (0.453, 0.515) for the series of Rh6G@MOF-5 composites (0–1×10^{-2} mol/L Rh6G levels) (Fig. 2B). The CIE coordinates moved from the blue region to the orange region with the increase of embedded Rh6G molecules, which was consistent with the emission color of Rh6G@ MOF-5 under UV light. All the above results further demonstrated that Rh6G molecules are uniformly linked to the channels of MOF-5 through covalent bonding as a modulator, since almost no significant color change was shown after several washes, thus the formation of aggregates in the solid state was inhibited.

Three fluorescence peaks were identified from the 3-D front-face fluorescence spectra of Rh6G@MOF-5. Excitation/Emission (Ex/Em) peak located at 330 nm/430 nm was attributed to MOF-5, Ex/Em peaks located at 350 nm/570 nm and 530 nm/570 nm were attributed to Rh6G (Fig. 3). It is found that fluorescence intensities of 350 nm/570 nm Rh6G peak was positively correlated with the amount of fluorescein. However, once the addition of Rh6G reached 1×10^{-2} mol/L, obvious fluorescence quenching located at 530 nm/570 nm was noticed, which was in accordance with the ACQ phenomenon of the free dye molecules (Fig. S3A). Based on that, the optimal amount of Rh6G was set at 1×10^{-3} mol/L to provide sufficient active sites and simultaneously protect Rh6G against a potential ACQ phenomenon for further experiments.

In order to further explore the interaction of Rh6G fluorescein and MOF-5 in this nanocomposite, the fluorescence decay curves of both Rh6G and the Rh6G@MOF-5 composite were measured. As Fig. 2C displayed, after embedding Rh6G molecules into the cavities of MOF-5, the fluorescence lifetime of Rh6G increased from 1.82 to 5.20 ns. The decrease in aggregation and deprotonation of Rh6G molecules after encapsulation into the MOF-5 framework was considered to increase the lifetime of Rh6G@MOF-5. The lifetime-prolonging Rh6G@MOF-5

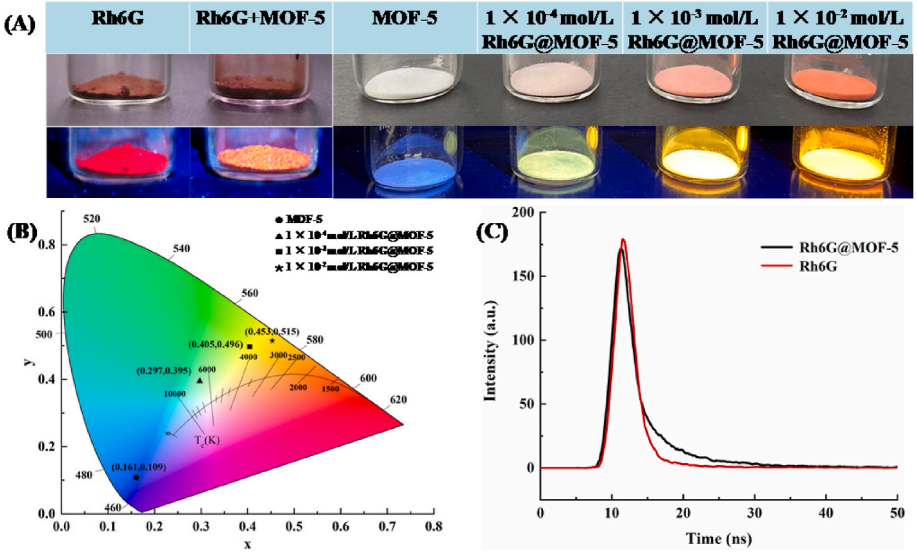

Fig. 2. (A) Photographs of Rh6G, Rh6G + MOF-5, MOF-5 and Rh6G@MOF-5 with different Rh6G concentrations under visual light and 365 nm UV light. (B) CIE chromaticity coordinates for Rh6G@MOF-5 with different Rh6G concentrations. (C) Time-resolved fluorescence decay curves of Rh6G and Rh6G@MOF-5.

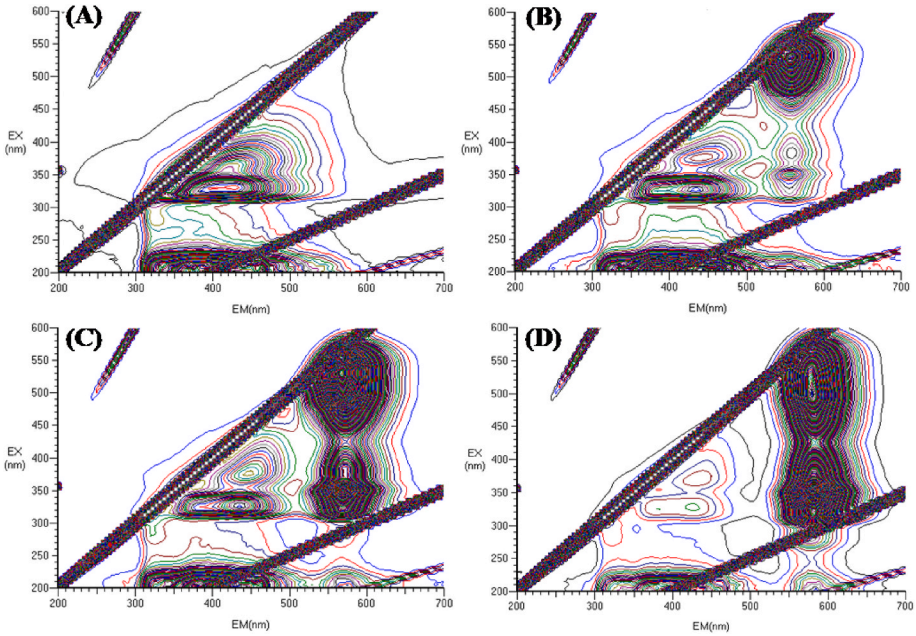

Fig. 3. The 3D-fluorescence spectra of MOF-5 (A), 10^{-4} Rh6G@MOF-5 (B), 10^{-3} Rh6G@MOF-5 (C) and 10^{-2} Rh6G@MOF-5 (D) solid powders.

hybrid showed significant advantages for practical applications of this LMOF in sensing (Guo, Liu, Kong, Chen, Liu, et al., 2019).

3.3. Optimization of detection condition

Generally, the rhodamine derivative displays a non-fluorescence spirolactam structure in neutral or alkaline conditions, yet shows a strong fluorescence xanthene structure in acidic conditions. This xanthenes structure may react with NO_2^-, thus displaying a sensing signal via quenching its emission (Wu & Nie, 2015). Moreover, nitrite sensing is frequently performed in an acidic solution so that sensing molecules are able to react with NO_2^- fully. As a consequence, a suitable acidic medium (HCl concentration) is necessary to be considered for ensuring this sensing process. Emission quenching (F_0–F) of Rh6G@MOF-5

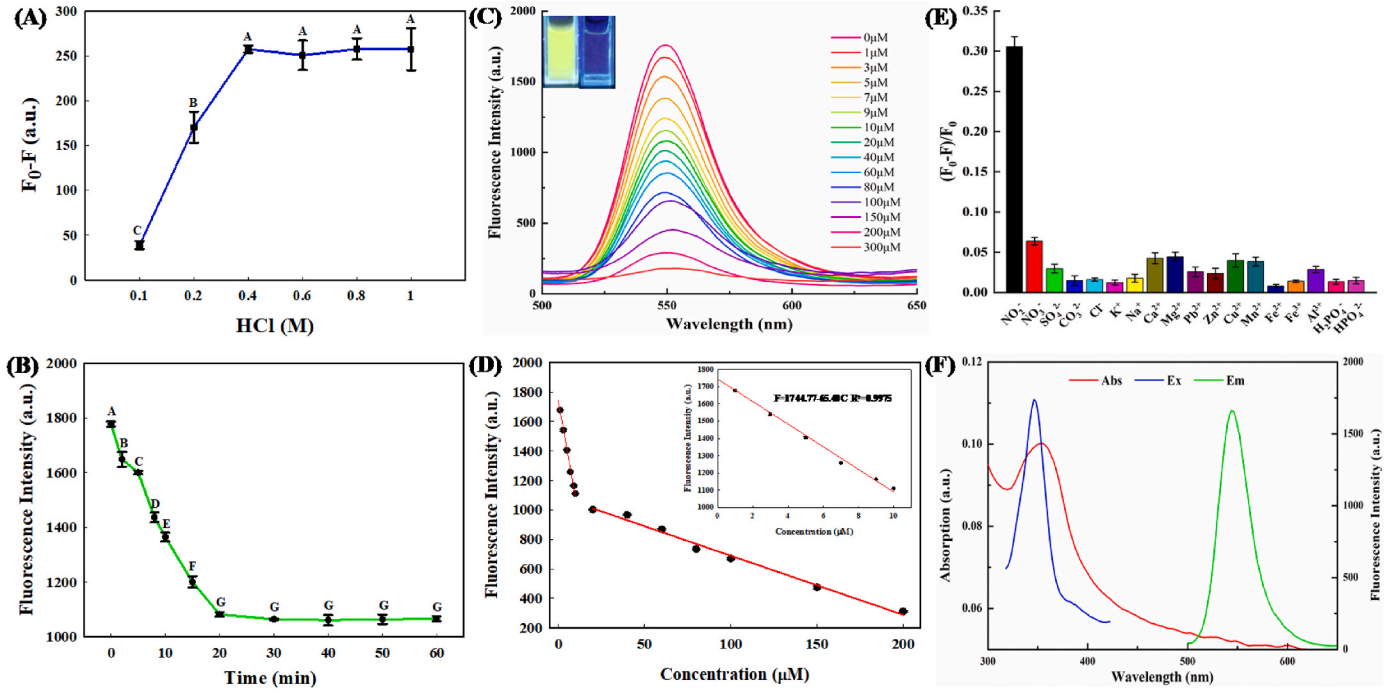

Fig. 4. (A) Effect of HCl concentration on the Rh6G@MOF-5-based sensor for nitrite (10 μM). F_0 means initial emission intensity without nitrite ion and F means emission intensity after adding nitrite ion. (B) Fluorescence intensity of Rh6G@MOF-5 suspension after reaction with nitrite (10 μM) for different times. (C) Evolvement of the fluorescence emission spectra of the Rh6G@MOF-5 suspension under various concentrations of nitrite (0–300 μM). Inset shows the corresponding photos of Rh6G@MOF-5 in the absence (left) and presence (right) of 1 mmol/L nitrite ion under 365 nm UV light. (D) Standard curve for the determination of nitrite concentration. (E) Fluorescence quenching efficiency ((F_0–F)/F_0) of the Rh6G@MOF-5 system containing different potential inteferences (NO_3^-, SO_4^{2-}, CO_3^{2-}, Cl^-, K^+, Na^+, Ca^{2+}, Mg^{2+}, Pb^{2+}, Zn^{2+}, Cu^{2+}, Mn^{2+}, Fe^{2+}, Fe^{3+}, Al^{3+}, $H_2PO_4^-$ and HPO_4^{2-}). The concentration of NO_2^- is 10 μM. The concentration of all other interferences are 100 μM. (F) UV–vis absorption of NO_2^-, fluorescence excitation and emission of Rh6G@MOF-5.

suspension under various HCl concentrations was shown in Fig. 4A. Notably, fluorescence quenching values increase obviously with increasing HCl concentrations from 0 mol/L to 0.4 mol/L, which may be attributed to the fact that protons accelerated the reaction between NO_2^- and Rh6G@MOF-5. Then, F_0–F values become smooth and non-fluctuating with increasing HCl concentrations from 0.4 mol/L to 1.0 mol/L. Hence, the optimal acid condition was chosen as 0.4 mol/L HCl concentration in this work since its fluorescence quenching achieved both maximum probe quenching and stable signal.

In addition, reaction time is another optimized factor to completely react and quench between nitrite ions and the Rh6G@MOF-5 sensing probe. To display the response time of Rh6G@MOF-5 toward nitrite, their fluorescence intensity variation was summarized in Fig. 4B. After the addition of the nitrite solution to the Rh6G@MOF-5 suspension, in its initial 20 min, the fluorescence intensities of the probe decreased rapidly, then this fluorescence quenching became smooth and the sensing process finally achieved equilibrium after 20 min. Therefore, 20 min was chosen as the optimal reaction time, indicating that maximum quenching can be achieved within 20 min. This fluorescence response time was slightly shorter than previous reports since the uniform and porous structure of synthesized MOF-5 could improve analyte diffusion and promote the interaction of nitrite with the fluorescent recognition site (Hu, Deibert, & Li, 2014; Huang, Ye, Zhao, Li, & Gu, 2019).

3.4. Fluorescence detection for nitrite based on Rh6G@MOF-5 sensor

The fluorescence intensity of the chemo-synthesized Rh6G@MOF-5 system in the presence of various NO_2^- concentrations ranging from 0 mmol/L to 300 mmol/L was recorded using the above suitable conditions (Fig. 4C). It was clear that the fluorescence emission peaking at 545 nm is quenched gradually as the nitrite ion concentration increases. As shown in Fig. 4D, a well linear relationship ($F = 1744.77–65.40\ C$, $R^2 = 0.9975$) was obtained between fluorescence intensity and NO_2^- concentration ranging from 1 μmol/L to 10 μmol/L. Furthermore, the limitation of detection (LOD) was defined as 3σ/s, where σ is the standard deviation of blank measurements and s is the slope of the linear calibration plot, respectively (Guo, Liu, Kong, Chen, Wang, et al., 2019). The LOD of nitrite ion obtained by the method reported herein was calculated to be 0.2 μmol/L, it is far below the ceiling concentration of NO_2^- in meat products (Zhang et al., 2016). The above results suggest that this sensitive Rh6G@MOF-5 fluorescence probe can be applied for efficient detection of nitrite ions in meat samples. Fig. S4 also showed a strong and positive correlation between NO_2^- concentration and fluorescence intensity in the range of 20–200 μmol/L ($R^2 > 0.990$). Furthermore, compared with the previously reported methods in nitrite detection, the LOD, detecting range, and response time of this LMOF probe are outperforming or close to the most reported sensors. Because the large specific surface area of porous material not only accommodates more identified probes but also enhances local concentration of nitrite ion recognition sites (Xie et al., 2020; Zhang et al., 2016) (Table S1). It's further confirmed that the proposed probe demonstrated excellent sensitivity and reliability for the detection of NO_2^- in the sensing system.

3.5. Anti-interference performance of Rh6G@MOF-5

Apart from sensitivity, the anti-interference is deemed another vital factor in evaluating the luminescent probe when detecting nitrite ions in a complex meat product system. Hence, the selectivity of the Rh6G@MOF-5 nanosensor platform toward NO_2^- was investigated. The possibly competitive interferences in meat samples, such as NO_3^-, SO_4^{2-}, CO_3^{2-}, Cl^-, K^+, Na^+, Ca^{2+}, Mg^{2+}, Pb^{2+}, Zn^{2+}, Cu^{2+}, Mn^{2+}, Fe^{2+}, Fe^{3+}, Al^{3+}, $H_2PO_4^-$ and HPO_4^{2-}, were added to test the selective performance of Rh6G@MOF-5 under the same conditions (Fig. 4E). Even though the added concentration of seventeen different interference ions (1×10^{-4} mol/L) was 10 times that of NO_2^- in the detection system, only NO_2^- treatment (1×10^{-5} mol/L) displays an obvious enhancement on the $(F_0–F)/F_0$ of the Rh6G@MOF-5 suspension, indicating that Rh6G@MOF-5 nanosensor has a great anti-interference capability and was not disturbed by other competitive ions. Due to the low LOD, wide detection range, high sensitivity, and great specificity toward NO_2^-, this LMOF could serve as an efficient NO_2^- detection plateform with high accuracy in meat product system.

3.6. Application in meat products

To assess the potential feasibility of the synthesized LMOF fluorescent sensor in complex meat products, six kinds of meat samples, including sausage, bacon, ham, and spiced meat products, were tested for NO_2^- determination. In the light of the procedure of the standardization method (GB 5009.33–2016), the NO_2^- was extracted from the above samples, different concentrations of NO_2^- standard solution were added, and the same method was used to estimate the recovery. As shown in Table 1, the obtained results did not demonstrate a significant difference with standard addition concentrations. The nitrite contents of sausage, bacon, pork ham, beef ham, spiced beef, and spiced chicken were 7.83 mg/kg, 6.45 mg/kg, 9.03 mg/kg, 7.45 mg/kg, 7.66 mg/kg and 3.81 mg/kg, respectively. The calculated quantitative recoveries of nitrite ranged from 96.1% to 103.20% with RSDs of less than 4%, indicating the designed probe's high analytical accuracy, precision, and reliability for the real-time detection of NO_2^- in meat products. Therefore, the Rh6G@MOF-5 could be an efficient and potential novel nanosensor platform for the NO_2^- recognition assay in actual application.

3.7. Sensing mechanism for the analysis of NO_2^-

In view of better understanding the origin of the excellent NO_2^--sensing ability of Rh6G@MOF-5, the possible synthesis approach and fluorescence quenching mechanism of the Rh6G@MOF-5 sensing platform were investigated and expressed in Scheme. Therefore, the optical properties of NO_2^- and the LMOF sensor were first compared. The UV–Vis absorption of NO_2^- and the fluorescence Ex and Em spectrum of Rh6G@MOF-5 were displayed in Fig. 4F. It is clear that NO_2^- had a characteristic UV–Vis absorption spectrum with a wide range from 320 to 500 nm. The absorption peak overlapped with the Ex peak (350 nm) of Rh6G@MOF-5, however, no significant overlap was observed between the Em spectrum of Rh6G@MOF-5 and the absorption spectrum of NO_2^-, suggesting that the quenched fluorescence of Rh6G@MOF-5 by NO_2^- might result from IFE rather than Förster resonance energy transfer (FRET) (Cheng, Tang, Zhang, Wu, & Yang, 2021). Previous literatures have displayed that the emission quenching between nitrite and Rh6G-based nanosensor could be ascribed to a static quenching

Table 1
Nitrite Determination in meat product samples by Rh6G@MOF-5 sensor system.

Samples	Added (mg/kg)	Found (mg/kg)	RSD (%, n = 3)	Recovery (%, n = 3)
Sausages	0.00	7.83	3.29	–
	13.80	14.47	2.87	96.1
	27.60	21.79	0.49	101.1
Bacon	0.00	6.45	3.88	–
	13.80	13.45	0.81	101.5
	27.60	20.18	1.74	99.4
Pork ham	0.00	9.03	2.70	–
	13.80	16.15	1.29	103.2
	27.60	22.46	2.46	97.3
Beef ham	0.00	7.45	1.63	–
	13.80	14.54	2.39	102.8
	27.60	21.46	0.58	101.5
Spiced beef	0.00	7.66	3.21	–
	13.80	14.62	1.21	100.9
	27.60	21.03	0.59	96.9
Spiced chicken	0.00	3.81	3.29	–
	13.80	10.72	1.69	100.2
	27.60	17.27	2.06	97.6

mechanism, which is consistent with our conclusion since IFE belonged to a static quenching process (Dhanya, Joy, & Rao, 2012; Zhang et al., 2016). The interaction of NO_2^- with Rh6G entrapped MOF-5 structure, on the other hand, depended on electron-withdrawing effect, namely, nitrosyl cation (NO^+) formed from NO_2^- in acid medium and the attack of electron deficient NO^+ with secondary amine group of Rh6G, resulting in the formation of nitroso group derivative, which quenched the representative fluorescence of rhodamine to some extent (Scheme B) (Viboonratanasri, Pabchanda, & Prompinit, 2018; Wang, Li, Zhang, Zhang, & Zhao, 2012; Zhang et al., 2016).

4. Conclusions

To summarize, a hybrid and functionalized LMOF composite (Rh6G@MOF-5) was synthesized by encapsulating organic dye Rh6G into the porous crystalline Zn (II)-MOF-5 by a facile solvothermal approach. This "Turn−off" mode nanoprobe exhibited better sensing performance, such as excellent selectivity, a low detection limit (0.2 μmol/L), and a short response time (20 min) toward nitrite. Furthermore, Rh6G@MOF-5 not only served as a regulator for nitrite determination but also prolonged the fluorescence lifetime of Rh6G. It is worth noting that this nanocomposite presents high reliability, sensitivity, and convenience for nitrite detection for meat product testing. Therefore, it may be a promising candidate for the detection of nitrite ions in complex food systems or supply effective guidance to design dye-loading LMOF materials for trace substance detection.

CRediT authorship contribution statement

Siyang Deng: Methodology, Software, Validation, Formal analysis, Investigation, Writing – original draft. **Huan Liu:** Formal analysis, Investigation, Writing – review & editing. **Chunhui Zhang:** Supervision, Project administration, Funding acquisition. **Xinting Yang:** Funding acquisition. **Christophe Blecker:** Supervision.

Declaration of competing interest

The authors declare that they have no known competing financial interests of personal relationships that could have appeared to influence the work reported in this paper.

Data availability

The authors do not have permission to share data.

Acknowledgement

This project was supported by a research grant from Special Fund of National Key R&D Program of China (grant no. 2021YFD2100103), Key scientific and technological projects of Xinjiang production and Construction Corps (grant no. 2020AB012) and the National Natural Science Foundation of China (32001775).

Appendix A. Supplementary data

Supplementary data to this article can be found online at https://doi.org/10.1016/j.lwt.2022.114030.

References

Brender, J., Olive, J., Felkner, M., Suarez, L., Hendricks, K., & Marckwardt, W. (2004). Intake of nitrates and nitrites and birth defects in offspring. *Epidemiology, 15*(4), S148.

Canbay, E., Şahin, B., Kıran, M., & Akyilmaz, E. (2015). MWCNT–cysteamine–Nafion modified gold electrode based on myoglobin for determination of hydrogen peroxide and nitrite. *Bioelectrochemistry, 101*, 126–131.

Cheng, W., Tang, X., Zhang, Y., Wu, D., & Yang, W. (2021). Applications of metal-organic framework (MOF)-based sensors for food safety: Enhancing mechanisms and recent advances. *Trends in Food Science & Technology, 112*, 268–282.

Dhanya, S., Joy, J., & Rao, T. P. (2012). Fabrication and characterization of rhodamine 6G entrapped sol-gel film test strip for virtually specific and sensitive sensing of nitrite. *Sensors and Actuators B: Chemical, 173*, 510–516.

Furukawa, H., Cordova, K. E., O'Keeffe, M., & Yaghi, O. M. (2013). The chemistry and applications of metal-organic frameworks. *Science, 341*(6149), 974.

Greer, F. R., & Shannon, M. (2005). Infant methemoglobinemia: The role of dietary nitrate in food and water. *Pediatrics, 116*(3), 784–786.

Guo, L., Liu, Y., Kong, R., Chen, G., Liu, Z., Qu, F., et al. (2019). A metal-organic framework as selectivity regulator for Fe^{3+} and ascorbic acid detection. *Analytical Chemistry, 91*(19), 12453–12460.

Guo, L., Liu, Y., Kong, R., Chen, G., Wang, H., Wang, X., et al. (2019). Turn-on fluorescence detection of β-glucuronidase using RhB@MOF-5 as an ultrasensitive nanoprobe. *Sensors and Actuators B: Chemical, 295*, 1–6.

Huang, C., Ye, Y., Zhao, L., Li, Y., & Gu, J. (2019). One-pot trapping luminescent rhodamine 110 into the cage of MOF-801 for nitrite detection in aqueous solution. *Journal of Inorganic and Organometallic Polymers and Materials, 29*(5), 1476–1484.

Hu, Z., Deibert, B. J., & Li, J. (2014). Luminescent metal–organic frameworks for chemical sensing and explosive detection. *Chemical Society Reviews, 43*(16), 5815–5840.

Hu, X., Shi, J., Shi, Y., Zou, X., Arslan, M., Zhang, W., et al. (2019). Use of a smartphone for visual detection of melamine in milk based on Au@Carbon quantum dots nanocomposites. *Food Chemistry, 272*, 58–65.

Hu, Y., Yang, H., Wang, R., & Duan, M. (2021). Fabricating Ag@MOF-5 nanoplates by the template of MOF-5 and evaluating its antibacterial activity. *Colloids and Surfaces A: Physicochemical and Engineering Aspects, 626*, Article 127093.

Kilfoy, B. A., Zhang, Y., Park, Y., Holford, T. R., Schatzkin, A., Hollenbeck, A., et al. (2011). Dietary nitrate and nitrite and the risk of thyroid cancer in the NIH-AARP Diet and Health Study. *International Journal of Cancer, 129*(1), 160–172.

Lee, K. S., Shiddiky, M. J. A., Park, S. H., Park, D. S., & Shim, Y. B. (2008). Electrophoretic analysis of food dyes using a miniaturized microfluidic system. *Electrophoresis, 29*(9), 1910–1917.

Let, S., Samanta, P., Dutta, S., & Ghosh, S. K. (2020). A dye@MOF composite as luminescent sensory material for selective and sensitive recognition of Fe(III) ions in water. *Inorganica Chimica Acta, 500*, Article 119205.

Li, H., Meininger, C. J., & Wu, G. (2000). Rapid determination of nitrite by reversed-phase high-performance liquid chromatography with fluorescence detection. *Journal of Chromatography B: Biomedical Sciences and Applications, 746*(2), 199–207.

Liu, H., Guo, K., Lv, J., Gao, Y., Duan, C., Deng, L., et al. (2017). A novel nitrite biosensor based on the direct electrochemistry of horseradish peroxidase immobilized on porous Co_3O_4 nanosheets and reduced graphene oxide composite modified electrode. *Sensors and Actuators B: Chemical, 238*, 249–256.

Liu, L., Yao, Z., Ye, Y., Liu, C., Lin, Q., Chen, S., et al. (2019). Enhancement of intrinsic proton conductivity and aniline sensitivity by introducing dye molecules into the MOF channel. *ACS Applied Materials & Interfaces, 11*(18), 16490–16495.

Maia, L. B., & Moura, J. J. G. (2014). How biology handles nitrite. *Chemical Reviews, 114*(10), 5273–5357.

Merusi, C., Corradini, C., Cavazza, A., Borromei, C., & Salvadeo, P. (2010). Determination of nitrates, nitrites and oxalates in food products by capillary electrophoresis with pH-dependent electroosmotic flow reversal. *Food Chemistry, 120*(2), 615–620.

Nam, J., Jung, I. B., Kim, B., Lee, S. M., Kim, S. E., Lee, K. N., et al. (2018). A colorimetric hydrogel biosensor for rapid detection of nitrite ions. *Sensors and Actuators B: Chemical, 270*, 112–118.

Pérez-López, M., De la Casa-Resino, I., Hernández-Moreno, D., Galeano, J., Míguez-Santiyán, M. P., de Castro-Lorenzo, A., et al. (2016). Concentrations of metals, metalloids, and chlorinated pollutants in blood and plasma of white stork (Ciconia ciconia) nestlings from Spain. *Archives of Environmental Contamination and Toxicology, 71*(3), 313–321.

Petit, C., & Bandosz, T. J. (2009). MOF–graphite oxide nanocomposites: Surface characterization and evaluation as adsorbents of ammonia. *Journal of Materials Chemistry, 19*(36), 6521–6528.

Sahiner, N., Demirci, S., & Yildiz, M. (2017). Synthesis and characterization of terephthalic acid based Cr^{3+}, Sb^{3+}, In^{3+} and V^{3+} metal-organic frameworks. *Journal of Inorganic and Organometallic Polymers and Materials, 27*(5), 1333–1341.

Santarelli, R. L., Vendeuvre, J. L., Naud, N., Taché, S., Guéraud, F., Viau, M., et al. (2010). Meat processing and colon carcinogenesis: Cooked, nitrite-treated, and oxidized high-heme cured meat promotes mucin-depleted foci in rats. *Cancer Prevention Research, 3*(7), 852–864.

Viboonratanasri, D., Pabchanda, S., & Prompinit, P. (2018). Rapid and simple preparation of rhodamine 6G loaded HY zeolite for highly selective nitrite detection. *Applied Surface Science, 440*, 1261–1268.

Wang, L., Li, B., Zhang, L., Zhang, L., & Zhao, H. (2012). Fabrication and characterization of a fluorescent sensor based on Rh 6G-functionlized silica nanoparticles for nitrite ion detection. *Sensors and Actuators B: Chemical, 171–172*, 946–953.

Wang, Q., Ma, S., Huang, H., Cao, A., Li, M., & He, L. (2016). Highly sensitive and selective spectrofluorimetric determination of nitrite in food products with a novel fluorogenic probe. *Food Control, 63*, 117–121.

Wang, B. H., & Yan, B. (2019). A dye@MOF crystalline probe serving as a platform for ratiometric sensing trichloroacetic acid (TCA), the metabolite of carcinogen in the human urine. *CrystEngComm, 21*, 4637–4643.

Wan, Y., Zheng, Y. F., Wan, H. T., Yin, H. Y., & Song, X. C. (2017). A novel electrochemical sensor based on Ag nanoparticles decorated multi-walled carbon nanotubes for applied determination of nitrite. *Food Control, 73*, 1507–1513.

Wu, Y. C., & Nie, F. (2015). A core–shell structured nanocomposite modified with rhodamine derivative for nitrite ion sensing. *Sensors and Actuators B: Chemical, 212*, 120–126.

Xie, X., Huang, X., Lin, W., Chen, Y., Lang, X., Wang, Y., et al. (2020). Selective adsorption of cationic dyes for stable metal–organic framework ZJU-48. *ACS Omega, 5*(23), 13595–13600.

Ye, Y., Zhao, L., Hu, S., Liang, A., Li, Y., Zhuang, Q., et al. (2019). Specific detection of hypochlorite based on the size-selective effect of luminophore integrated MOF-801 synthesized by a one-pot strategy. *Dalton Transactions, 48*(8), 2617–2625.

Zhang, Y., Su, Z., Li, B., Zhang, L., Fan, D., & Ma, H. (2016). Recyclable magnetic mesoporous nanocomposite with improved sensing performance toward nitrite. *ACS Applied Materials & Interfaces, 8*(19), 12344–12351.

Zheng, X. J., Liang, R. P., Li, Z. J., Zhang, L., & Qiu, J. D. (2016). One-step, stabilizer-free and green synthesis of Cu nanoclusters as fluorescent probes for sensitive and selective detection of nitrite ions. *Sensors and Actuators B: Chemical, 230*, 314–319.

Zhou, L., Anwar, M. M., Zahid, M., Shostrom, V., & Mirvish, S. S. (2014). Urinary excretion of N-nitroso compounds in rats fed sodium nitrite and/or hot dogs. *Chemical Research in Toxicology, 27*(10), 1669–1674.